Article

Cell Reports

Sensory Afferents Use Different Coding Strategies for Heat and Cold

Graphical Abstract

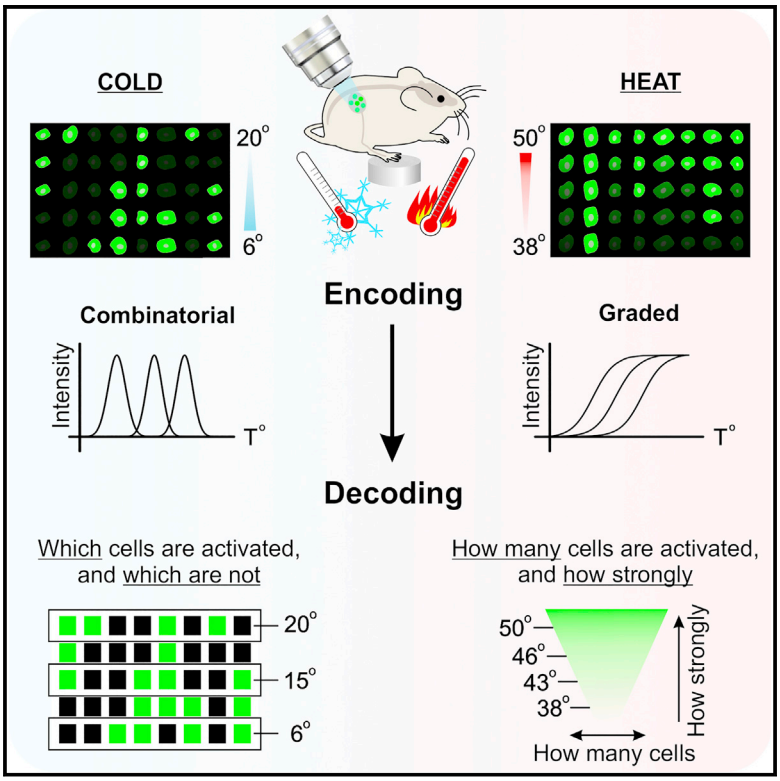

Highlights

- Ca^{2+} imaging yields sufficient sensitivity to resolve all sensory modalities in DRGs
- Unbiased imaging from large populations reveals >50% sensory neurons are polymodal
- Heating- and cooling-sensitive neurons have distinct tuning curves
- Graded coding prevails for heat versus combinatorial coding for cold

Authors

Feng Wang, Erik Bélanger, Sylvain L. Côté, Patrick Desrosiers, Steven A. Prescott, Daniel C. Côté, Yves De Koninck

Correspondence

yves.dekoninck@neuro.ulaval.ca

In Brief

Wang et al. imaged thousands of mouse DRG neurons *in vivo*. They found the majority of small neurons to be polymodal. Furthermore, heat is encoded in a graded fashion by both individual and the population of neurons, whereas cold is encoded by the population of neurons using a combinatorial strategy.

Wang et al., 2018, Cell Reports *23*, 2001–2013
May 15, 2018
https://doi.org/10.1016/j.celrep.2018.04.065

CellPress

Cell Reports
Article

Sensory Afferents Use Different Coding Strategies for Heat and Cold

Feng Wang,[1,7] Erik Bélanger,[1,2,7] Sylvain L. Côté,[1] Patrick Desrosiers,[1,3] Steven A. Prescott,[4,5] Daniel C. Côté,[1,2,3] and Yves De Koninck[1,2,6,8,*]
[1]CERVO Brain Research Centre, Québec Mental Health Institute, Quebec City, QC, Canada
[2]Center for Optics, Photonics and Lasers (COPL), Laval University, Quebec City, QC, Canada
[3]Department of Physics, Physical Engineering, and Optics, Laval University, Quebec City, QC, Canada
[4]Neurosciences and Mental Health, The Hospital for Sick Children, Toronto, ON, Canada
[5]Department of Physiology and the Institute of Biomaterials and Biomedical Engineering, University of Toronto, Toronto, ON, Canada
[6]Department of Psychiatry and Neuroscience, Laval University, Quebec City, QC, Canada
[7]These authors contributed equally
[8]Lead Contact
*Correspondence: yves.dekoninck@neuro.ulaval.ca
https://doi.org/10.1016/j.celrep.2018.04.065

SUMMARY

Primary afferents transduce environmental stimuli into electrical activity that is transmitted centrally to be decoded into corresponding sensations. However, it remains unknown how afferent populations encode different somatosensory inputs. To address this, we performed two-photon Ca^{2+} imaging from thousands of dorsal root ganglion (DRG) neurons in anesthetized mice while applying mechanical and thermal stimuli to hind paws. We found that approximately half of all neurons are polymodal and that heat and cold are encoded very differently. As temperature increases, more heating-sensitive neurons are activated, and most individual neurons respond more strongly, consistent with graded coding at population and single-neuron levels, respectively. In contrast, most cooling-sensitive neurons respond in an ungraded fashion, inconsistent with graded coding and suggesting combinatorial coding, based on which neurons are co-activated. Although individual neurons may respond to multiple stimuli, our results show that different stimuli activate distinct combinations of diversely tuned neurons, enabling rich population-level coding.

INTRODUCTION

Dorsal root ganglion (DRG) neurons serve as the primary afferent neurons in the somatosensory system. They convert the physical and chemical state of the external and internal environment into neuronal activity and transmit this information to the CNS, where corresponding sensations are formed (Basbaum et al., 2009; Craig, 2002; Prescott et al., 2014). Sensation relies on the faithful encoding of stimuli by primary sensory neurons. However, how natural stimuli are represented by an ensemble of these neurons remains a subject of debate, with competing theories prevailing: combinatorial versus specificity theory (Ma, 2010; Perl, 2007; Prescott et al., 2014; Prescott and Ratté, 2012).

The specificity or labeled line theory posits that differently tuned sensory pathways are uniquely activated by distinct stimuli and that the corresponding sensation depends on which pathway is activated (Prescott et al., 2014). Support for the specificity theory includes results from behavioral studies using different transgenic mouse lines, where responsiveness to certain stimuli is selectively altered by the deletion/ablation of specific genes or cell types (Le Pichon and Chesler, 2014). For instance, deleting FGF13 in sensory neurons selectively abolishes heat pain but does not affect mechanical pain (Yang et al., 2017). Similarly, ablation of sensory neurons expressing TRPM8, a cold-activated channel, causes profound loss of cold sensation (Knowlton et al., 2013; Milenkovic et al., 2014; Pogorzala et al., 2013), whereas ablation of $MrgprD^{+}$ sensory neurons abolishes mechanical but not thermal pain (Cavanaugh et al., 2009). These results support the concept that selective populations of sensory neurons underlie specific sensory modalities.

Although the specificity theory holds that each neuron is activated by a specific type of stimulus, each stimulus may activate more than 1 neuron type but in unique combinations, according to combinatorial coding (Prescott et al., 2014; Prescott and Ratté, 2012). In other words, combinatorial coding hinges on which neurons are co-activated by a given stimulus, similar to trichromacy in the retina. The polymodality of DRG neurons is liable to facilitate combinatorial coding, whereas it is clearly a design flaw according to the specificity theory. The existence and prevalence of polymodal afferents is a pivotal issue in the debate between specificity theory and combinatorial coding theory. Evidence of polymodality comes from diverse electrophysiological recordings in primary afferent axons or somata from skin-nerve preparations, *in vivo* preparations in anesthetized animals, and human microneurography. Polymodal neurons have been identified in variable proportions depending

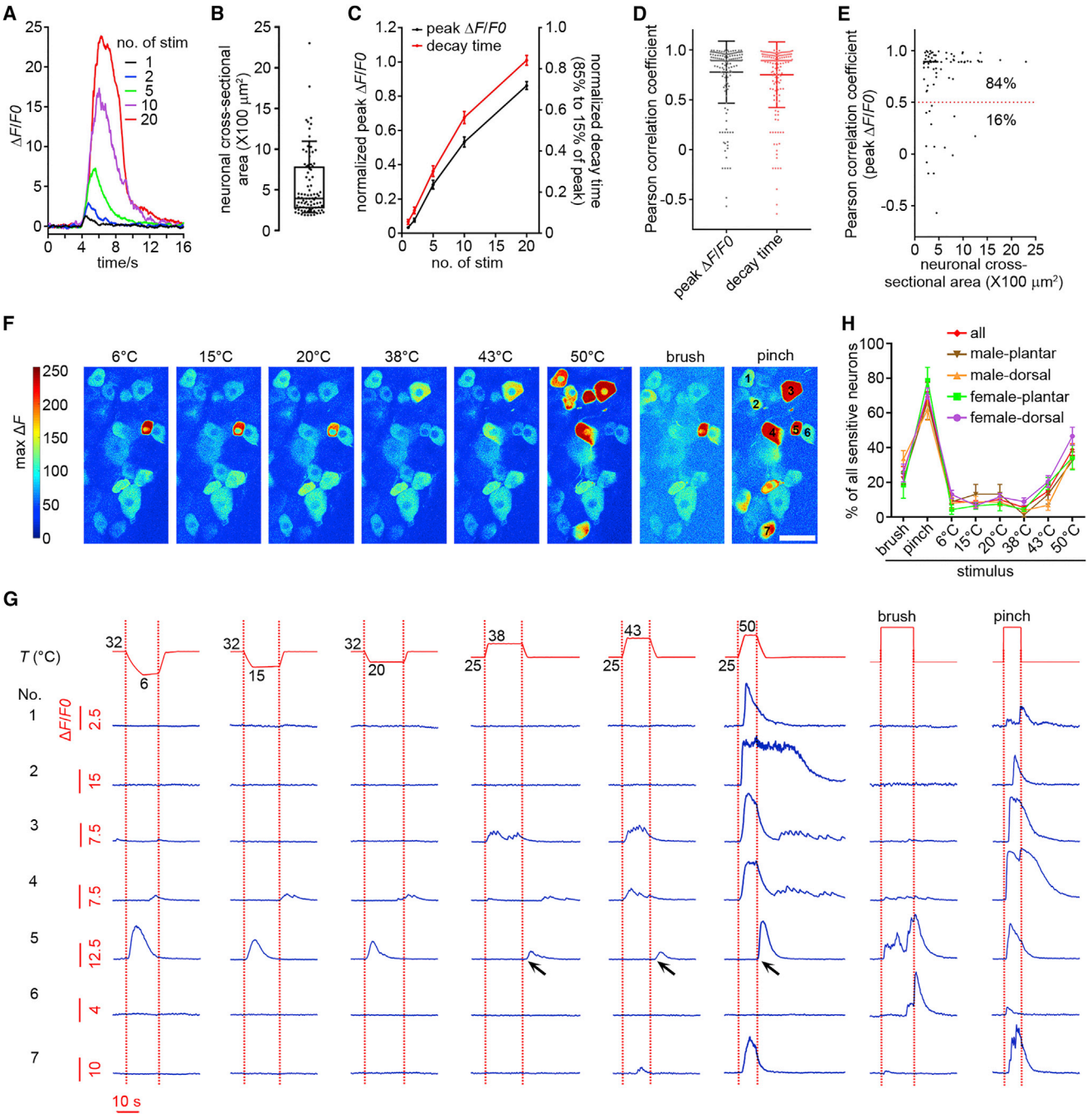

Figure 1. *In Vivo* Functional Imaging of Sensory Neurons

(A) Example of Ca^{2+} responses activated by different numbers of electrical pulses delivered to the exposed sciatic nerve.

(B) Distribution of cross-sectional areas of DRG neurons activated by 5 mA electrical stimulation showed that DRG neurons with different sizes could be activated. The box shows quartiles, and whiskers show 10–90 percentiles.

(C) Plots of the normalized peak amplitude (left y axis) and decay time (85% to 15% of peak, right y axis) of Ca^{2+} responses to different numbers of electrical stimuli. Data are presented as mean ± SEM.

(D) High linear correlation between Ca^{2+} responses and numbers of electrical stimuli in DRG neurons. Data are presented as mean ± SD.

(E) Good linear correlation is preserved across DRG neurons with different sizes. The Pearson correlation coefficient of 84% of neurons was above 0.5.

(F) Color-coded heatmap of a typical imaging field showing neuronal responses to noxious and innocuous thermal and mechanical stimuli. The color scale indicates maximum Δ*F*.

(G) Representative Ca^{2+} curves from seven neurons highlighted in (F) showing typical responses to thermal and mechanical stimuli. Note the different Δ*F*/*F0* scales for different neurons. Neuron 5 responded to cooling stimuli and to the return phase (black arrow) from heating stimuli but not to the onset of heating stimuli.

(legend continued on next page)

on species and tissue innervated (Beitel and Dubner, 1976; Bessou and Perl, 1969; Lynn and Carpenter, 1982; Torebjörk, 1985). In mice, polymodal afferents have been reported to represent 47% and 80% of the fibers innervating hairy and glabrous skin, respectively (Cain et al., 2001; Koltzenburg et al., 1997).

However, the polymodality of primary afferents was recently called into question by a study using *in vivo* Ca^{2+} imaging in mouse DRG neurons (Emery et al., 2016) that reported that most neurons responded to only one type of stimulus. Emery et al. (2016) suggested that polymodality was an artifact of injury during tissue preparation. Another potential limitation of electrophysiological experiments is their use of search stimuli, which can cause plastic changes over time. Beyond circumventing these potential limitations, imaging approaches also offer the advantage of recording from large numbers of cells to obtain unbiased population data. The study by Emery et al. (2016), however, imaged a relatively small set of neurons, and sampling may therefore be biased. Here we performed *in vivo* Ca^{2+} imaging in mouse DRGs using selective transduction of the genetically encoded Ca^{2+} indicator GCaMP6s into primary sensory neurons. Optical recording was performed using video-rate two-photon microscopy to ensure high spatial resolution and fast temporal sampling from individual neurons and from large sets of neurons. Consistent with electrophysiological studies, our results revealed that approximately half of all DRG neurons respond to more than one mechanical or thermal modality, with >30% responding to both mechanical and thermal stimuli. These results clearly demonstrate polymodality and support combinatorial coding.

To further test the type of encoding that prevails in afferents, we examined in more detail the distribution and dynamic responses of thermoceptive neurons. Parametric analysis of thermal responses from large sets of cells revealed that thermoceptive afferents use different strategies to encode heat and cold. Heat is encoded by how strongly each neuron is activated and, at the population level, by how many neurons are activated. This is enabled, respectively, by neurons having graded monotonic tuning curves and by the tuning curves of different neurons being distributed (staggered) across a range of temperatures. In contrast, cold is encoded by all-or-none activation of different neurons across different temperature ranges, which is enabled by most cooling-sensitive neurons having non-monotonic or steep monotonic tuning curves.

RESULTS

Unbiased Transduction of GCaMP6s across DRG Neuron Populations

To perform *in vivo* Ca^{2+} imaging from a random sample of all DRG cell types, we intraplantarly injected viral vectors encoding GCaMP6s (Chen et al., 2013) under the CAG promoter into wild-type mice (Figure S1A). Compared with non-transduced littermates, virally transduced mice did not show any significant difference in withdrawal latency or threshold (Figures S1B and S1C), indicating that expression of GCaMP6s did not affect thermal or mechanical sensation. Despite strong expression of GCaMP6s, its low basal fluorescence under *in vivo* condition without stimulation (Figure S1D) was ideal to yield a good dynamic range.

Expression of GCaMP6s verified that our approach transduced all types of DRG neurons in an unbiased manner. With or without antibody amplification, approximately 40% of DRG neurons in different subtypes displayed a clear GCaMP6s signal (Figure S2). We also found extensive distribution of $GCaMP6s^+$ fibers throughout all dorsal horn laminae, confirming transduction of a broad base of primary afferent cell types (Figure S3). In contrast, we did not find any $GCaMP6s^+$ spinal cord neurons (Figure S3C). Thus, intraplantar injection of AAV9 in newborn mice appears to selectively transduce DRG neurons but transduces all types of DRG neurons with comparable efficiency (Figure S2), implying that all types of afferents are well represented in the *in vivo* Ca^{2+} imaging we carried out.

In Vivo Ca^{2+} Imaging from Mouse DRG Neurons

We conducted *in vivo* video-rate two-photon functional imaging (Laffray et al., 2011) from L4 or L5 DRGs (primarily L4), which heavily innervate the hind paw (Figure S1A). To test whether GCaMP-based Ca^{2+} signals can reliably reflect the firing of DRG neurons, we first delivered different numbers of electrical stimuli at 5 Hz to the exposed sciatic nerve (Figures 1A–1E). Short (1 ms) electrical pulses at high intensity were used to activate all fiber types, as verified by the activation of different-size neurons (Figure 1B). The amplitude and decay time of Ca^{2+} responses showed no sign of saturation even at 20 stimuli (Figures 1A and 1C) and good linear correlation with the number of electrical stimuli (Figures 1C and 1D). Moreover, the linear correlation held across neurons of different sizes (Figure 1E), suggesting that the Ca^{2+} signal is a faithful proxy of firing for all types of DRG neurons.

Thermal stimuli were delivered to the hind paw with a thermal probe that covers one side of the whole paw. To characterize thermosensory representation globally, the responses of DRG neurons to a graded series of fast-ramp-and-hold thermal stimuli were recorded. The thermal stimuli covered innocuous cool to noxious cold as well as innocuous warm to noxious heat (Figures 1F and 1G). Upon active cooling or heating stimuli, robust and widespread Ca^{2+} responses were observed (Figures 1F and 1G). In general, a higher proportion of cells were heating-sensitive than cooling-sensitive (Figures 1G and 1H). We also noted that the cooling-sensitive neurons (e.g., neuron 5 in Figure 1G) were often sensitive to a decrease in temperature, and

Top: the protocols for fast-ramp-and-hold thermal stimuli as well as the onset and offset of manual brush and pinch stimulation. A baseline of 32°C and 25°C was chosen for cooling and heating stimuli, respectively. Multiple repeated brush or pinch stimuli were given in each trial of mechanical stimulation.
(H) Proportion of reactive neurons (i.e., that responded to at least one type of stimulus applied to the hind paw) in each imaging field that responded to different mechanical and thermal stimuli (n = 5 males for the dorsal paw, 2 males for the plantar paw, 6 females for the dorsal paw, and 3 females for the plantar paw). There was no statistical difference under different conditions using two-way repeated measures ANOVA. Data are presented as mean ± SEM.
See also Figures S1–S3.

a subset showed Ca^{2+} responses when the temperature returned to baseline after heating (see below).

To stimulate as many neurons as possible with mechanical stimuli, we applied repetitive gentle brush and pinch stimulation to the whole surface of the hind paw. As with thermal stimuli, brush and pinch stimuli induced robust Ca^{2+} responses. In general, we found a higher proportion of pinch-sensitive than brush-sensitive neurons (Figures 1G and 1H).

In total, 1477 neurons were tested with both mechanical and thermal stimuli applied to either the plantar or dorsal sides of the hind paw, in both male and female mice. Among these, 542 neurons responded to at least one type of stimulus. We did not observe significant differences in the proportion or the pattern of neuronal responses when stimulating the plantar versus dorsal side of the paw, nor between male and female mice (Figure 1H). Thus, we pooled these data. Of the 542 responsive neurons, 26% responded to brushing and 69% to pinching (Figure 1H). Between 8% and 10% of cells responded to cooling in the 6°C to 20°C range, and an increasing proportion of cells, from 5% to 38%, responded to heating from 38°C to 50°C (Figure 1H).

High Proportion of Polymodal Sensory Afferents

A substantial fraction of DRG neurons responded to at least two different types of stimulation (Figure 2A). For instance, 14% to 40% of pinch- or thermo-sensitive neurons also responded to brushing, whereas 50% to 75% of brush-sensitive or thermo-sensitive neurons were activated by pinching. Also, 17% to 40% of all mechano- and cooling-sensitive neurons responded to 50°C stimulation. However, <10% of mechano- and noxious heat-sensitive neurons responded to cooling stimuli (Figure 2A). The response patterns are similar in the neurons innervating the dorsal and plantar sides of the hind paw (Figures 2A1 and 2A2).

To better characterize the polymodality of cells, we categorized them into mechano-sensitive (responding to brushing or pinching), heating-sensitive (responding to 38°C, 43°C, or 50°C), and cooling-sensitive (responding to 6°C, 15°C, or 20°C). There was substantial overlap between mechano-sensitive and heating-sensitive neurons (Figure 2B). Approximately 34% of mechano-sensitive neurons responded to at least one type of heating stimulus, and 60% of heating-sensitive neurons responded to brushing or pinching. Similarly, a high percentage (57% and 43%) of cooling-sensitive neurons responded to mechanical and heating stimuli, respectively. In contrast, a relatively small percentage of mechano- (10%) or heating-sensitive (18%) neurons responded to cooling stimuli (Figure 2B). Furthermore, we applied the same analysis to neurons innervating the plantar and dorsal sides of the hind paw separately (Figures 2B1 and 2B2). We found a similar distribution of modalities on both sides of the paw, further justifying pooling of the data.

We also characterized the distribution of neuronal cell body size (Figure 2C). Unsupervised analysis revealed four modes in the size distribution. The first two modes (278 ± 63 μm^2 and 443 ± 113 μm^2) correspond to small neurons typically associated with C fibers (Molliver et al., 1997) but appear to represent two different populations with overlapping size distributions. The next two modes (772 ± 54 μm^2 and 1,062 ± 113 μm^2) correspond to medium and large-size neurons, respectively. We used 650 μm^2 and 900 μm^2 to separate small, medium, and large neurons. Most of the medium and large neurons were mechano-sensitive, whereas small neurons had complex response profiles encompassing all functional types (Figure 2D).

Then we subdivided neurons into distinct groups based on all possible combinations of response profiles (Figure 2E). The largest group represents neurons activated only by noxious pinching and comprised neurons of all sizes. The next largest groups represent neurons activated only by 50°C and neurons activated by both pinching and 50°C, both of which comprised mainly small neurons. The neurons that responded only to brushing or to both brushing and pinching also formed large groups and were distributed among small, medium, and large neurons. Neurons that responded to pinch, 43°C, and 50°C stimuli were mainly small cells. Neurons that responded to all cooling stimuli were among the smallest cells, regardless of whether they were mechano-sensitive. The remaining combinations of modalities (>50 categories) comprised very few neurons and were lumped together (Figure 2E, others).

We further analyzed the thermo-sensitivity of mechano-sensitive neurons (Figures 2F–2H). We found an extensive overlap between pinch-sensitive and heating-sensitive neurons (the majority responding to 50°C; Figures 2F and 2G). Also, >50% of cooling-sensitive neurons responded to pinching (Figure 2H). In contrast, <12% of mechano-sensitive neurons displayed cooling sensitivity (Figures 2B and 2H).

In conclusion, although most medium to large neurons were selectively mechano-sensitive, the majority of small neurons were polymodal and responded to multiple types of mechanical and thermal stimuli.

Thermal Coding: Graded versus Combinatorial

To more thoroughly characterize the thermal response profile of sensory afferents, we imaged more DRG neurons, focusing only on thermal stimuli. In total, we imaged 4,083 DRG neurons from 40 imaging fields in 29 animals. Among these, 674 neurons showed responses to at least one type of thermal stimulus. Among all identified thermoceptive neurons, the proportion responding to thermal stimuli was similar regardless of the stimulation site or sex (Figure 3A), and data were therefore pooled for further analysis. Approximately 15% of all thermoceptive neurons responded to 6°C, 15°C, or 20°C stimuli. On the other hand, approximately 10%, 20%, and 70% of all thermoceptive neurons responded to 38°C, 43°C, and 50°C, respectively (Figure 3A). As summarized in Figure 3C, the largest population comprised neurons activated only by 50°C (extreme heat neurons). The next largest group comprised neurons activated by both 50°C and 43°C. Neurons activated by all cooling stimuli (wide-range cool/cold neurons), all heating stimuli (wide-range warm/heat neurons), only 6°C, or only 15°C also formed sizeable groups. There were also 32 additional groups, each containing only a few neurons (<2%), that were lumped into "others." Most thermoceptive neurons were small cells, except those activated only by extreme heat, which were distributed among a wide spectrum of sizes (Figure 3C).

We then examined the spectrum of thermal sensitivity among the whole population of DRG neurons. Overall, two general

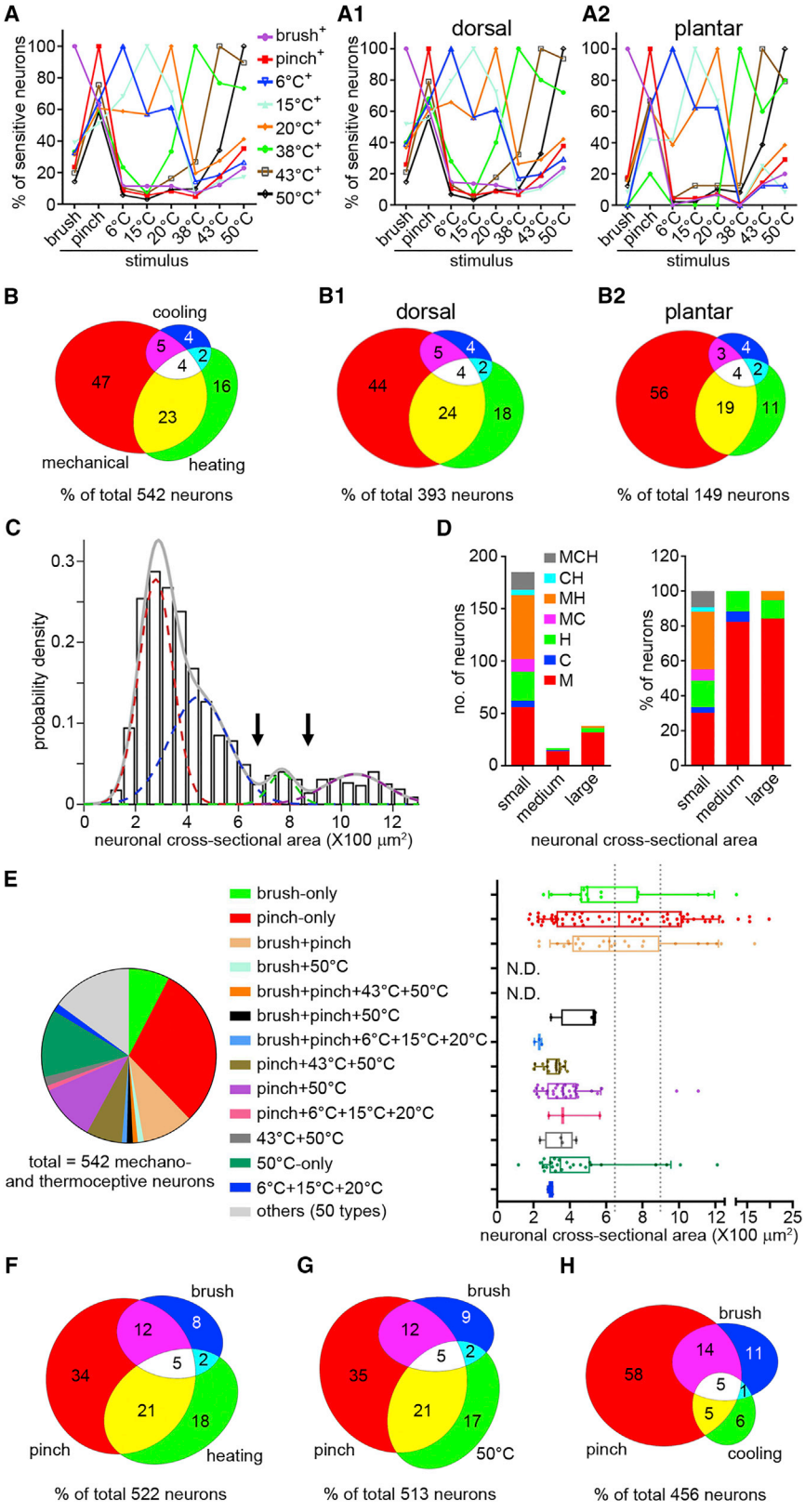

Figure 2. The Majority of Small Sensory Afferents Are Polymodal

(A) Proportion of neurons activated by a given stimulus (different lines) that responded to each type of mechanical and thermal stimulus. Also shown is the same analysis with data subdivided based on whether stimuli were applied to the dorsal side (A1) or plantar side (A2) of the hind paw.

(B) Euler diagram showing the overlap in distribution of mechano-sensitive (responsive to brushing or pinching), heating-sensitive (responsive to 38°C, 43°C, or 50°C), and cooling-sensitive neurons (responsive to 20°C, 15°C, or 6°C). Numbers indicated the percentage of a total of 542 mechanoceptive or thermoceptive neurons. Also shown is the same analysis with data subdivided based on whether stimuli were applied to the dorsal side (B1) or plantar side (B2) of the hind paw.

(C) Size distribution of sensory afferents (cross-sectional areas measured *in vivo* at the level of the nucleus) showed four modes using unsupervised fitting with Gaussian distributions. Arrows point to the thresholds used, based on the fitted distributions, to group neurons into three general categories in (D): small, medium, and large.

(D) Number (left) and proportion (right) of neurons with distinct mechanical and thermal sensitivity in the small, medium, and large categories, respectively, as defined in (C). M, mechano-sensitive; C, cooling-sensitive; H, heating-sensitive as defined in (B). More than half of the small neurons responded to multiple sensory modalities.

(E) Left: pie chart showing the distribution of neurons with a distinct response profile among all neurons that responded to stimulation of the hind paw. Right: distribution of neuronal size for each of the subgroups defined on the left. The "others" category contained 50 other types, each representing <2% of the whole population, that were thus lumped together. The box shows quartiles, and whiskers show 10–90 percentiles. N.D., not determined.

(F–H) Euler diagrams showing overlap in neurons responsive to the three types of stimuli: brush, pinch, as well as heating (F), 50°C (G), or cooling (H). Numbers indicate the percentage of a total of the neurons responding to at least one of the three types of stimuli, as indicated.

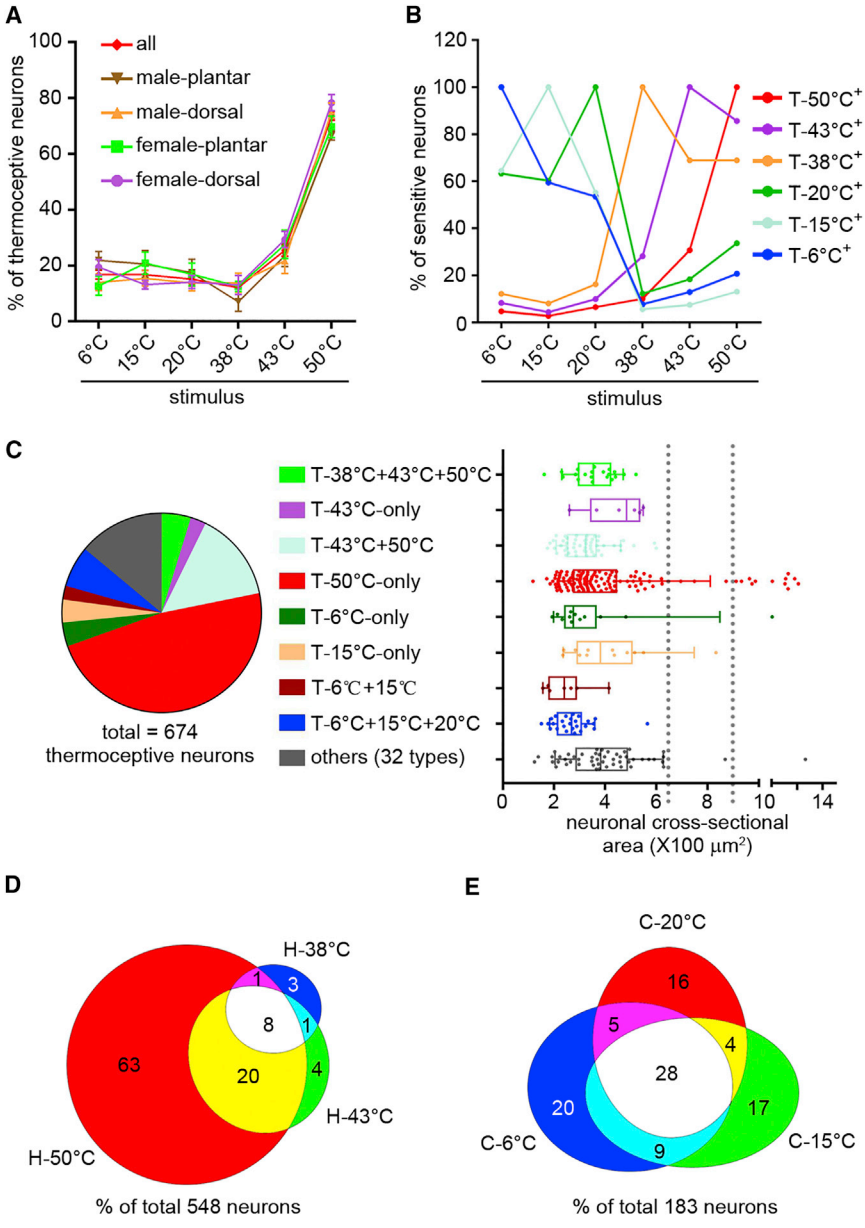

Figure 3. Thermoceptive Graded versus Combinatorial Coding

(A) Proportion of all thermoceptive neurons in each imaging field that responded to different thermal stimuli. There was no significant difference among the different groups (n = 13 males for the dorsal paw, 7 males for the plantar paw, 12 females for the dorsal paw, and 8 females for the plantar paw), using two-way repeated measures ANOVA. Data are presented as mean ± SEM.

(B) Proportion of neurons activated by a given stimulus (different lines) that responded to each type of thermal stimulus.

(C) Left: pie chart representation of the distribution of neurons with a distinct thermal sensitivity profile among all thermoceptive neurons. Right: distribution of neuronal size for each of the subgroups defined on the left. The "others" category contained 32 other types, each representing <2% of the whole population, that were thus lumped together. The box shows quartiles, and whiskers show 10–90 percentiles.

(D and E) Euler diagrams showing overlap in neurons responsive in the warm/heat (D) and cool/cold ranges (E). Numbers indicate the percentage of a total of the neurons responding to at least one of the three stimuli, as indicated.

thermoceptive profiles emerged: cells encoding mainly in the cooling range versus cells encoding in the heating range with minimal overlap, except for a small proportion of cooling-sensitive cells that responded to extreme heat (Figure 3B). We therefore examined in greater depth the overlap range in thermal sensitivity within each of those general thermoceptive profiles (cooling versus heating ranges). Striking differences between the heating-sensitive and cooling-sensitive groups emerged. In the heating range, the number of cells sensitive to higher temperatures increased (Figures 3A and 3D), but, more importantly, the group of cells sensitive to lower temperatures represented a nested subset of cells recruited at higher temperatures (Figure 3D). This reveals that, as temperature grows, an increasing number of cells are activated, thus enabling population-level graded coding of intensity. In contrast, in the cooling-sensitive group, many cells responded to a single temperature (6°C, 15°C, or 20°C; i.e., they were narrow-range), which, at a population level, precludes the progressive recruitment of neurons as the temperature was reduced (Figure 3A). Our analysis revealed three partially intersecting subsets of cooling-sensitive neurons (Figure 3E), inconsistent with graded coding and instead suggestive of combinatorial coding (see below).

Encoding in the Heating Range

To test whether thermoceptive neurons could individually encode stimulation intensity, we analyzed subsets of cells that responded to more than one temperature. Figure 4A shows typical responses of wide-range warm/heat neurons to 38°C, 43°C, and 50°C. More than 67% of wide-range warm/heat neurons exhibited graded responses to increasing temperatures (Figures 4A–4C). The Ca^{2+} responses were larger in peak amplitude and decayed slower back to baseline at higher temperatures (Figures 4B and 4C), but the rise time was insensitive to temperature (Figure 4D). Neurons responding to both 43°C and 50°C, but not 38°C (i.e., moderate-range), displayed similar graded responses between these two temperatures (Figures 4B–4D). These results demonstrate that individual neurons encode temperature across a moderate to wide range of elevated temperatures. The initial recruitment of wide-range neurons at 38°C and the additional recruitment of

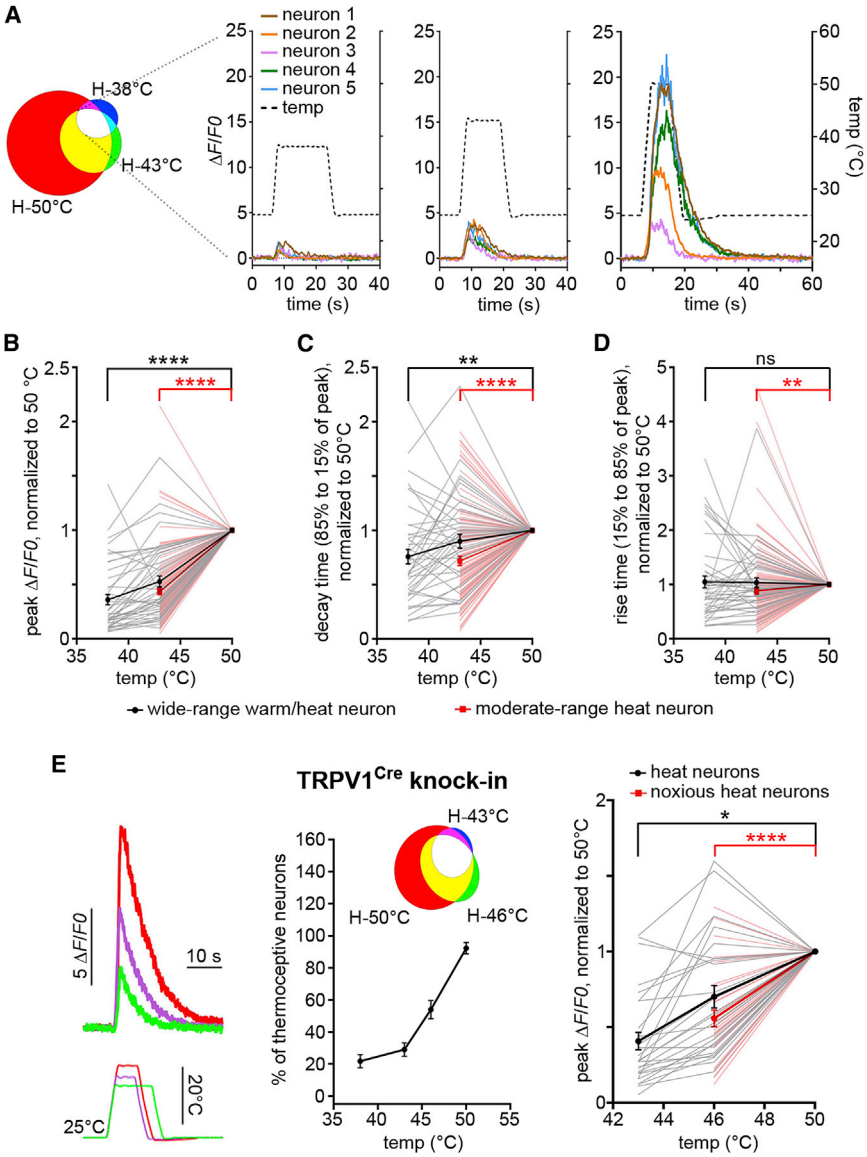

Figure 4. Individual Wide-Range Warm/Heat Neurons Provide Graded Coding

(A) Representative traces of Ca^{2+} responses of typical neurons that were sensitive to all heating stimuli (white overlap region in the Euler diagram) from 38°C to 50°C.

(B–D) Plots of the normalized peak amplitude (B), decay time (85% to 15% of the peak, C), and rise time (15% to 85% of the peak, D) of wide-range warm/heat neurons (gray curves, individual neuron response; black curve, mean response of the group) as well as moderate-range heat neurons (pale red curves, individual neuron response; red curve, mean response of the group) to increasing temperature. Both wide-range warm/heat and moderate-range heat neurons displayed significantly greater responses as the temperature increased (one-way repeated measures ANOVA test followed by Tukey's multiple comparisons test for wide-range warm/heat neurons and paired t test for moderate-range heat neurons). Data are presented as mean ± SEM.

(E) Response of GCaMP6s^{+} neurons from TRPV1^{Cre} knockin mice to noxious heat stimuli in the 43°C–50°C range. Left: representative response of the same neuron to 43°C, 46°C, and 50°C stimulation. Center: proportion of all GCaMP6s^{+} thermoceptive neurons from TRPV1^{Cre} knockin mice in each imaging field that responded to different thermal stimuli above 38°C. Inset: Euler diagram showing the overlap in neurons responsive in the heating range above 43°C. Right: these heat-sensitive neurons, both as a group (black for 43°C–50°C-responsive neurons, red for 46°C–50°C-responsive neurons) and individually (gray for 43°C–50°C-responsive neurons and pale red for 46°C–50°C-responsive neurons), displayed significantly greater responses with increasing temperature (one-way repeated measures ANOVA test followed by Tukey's multiple comparisons test for 43°C–50°C neurons; paired t test for 46°C–50°C neurons). Data are presented as mean ± SEM.

moderate-range neurons at 43°C is the basis for graded coding at the population level. In other words, more neurons are activated, and each neuron is activated more strongly as temperature is elevated, thus enabling graded coding by individual neurons and by the population as a whole.

To further explore graded coding in the noxious heat range, we used TRPV1^{Cre} knockin mice (Cavanaugh et al., 2011) as a tool, combined with viral transduction of Cre-dependent GCaMP6s to label an enriched subpopulation of heat-sensitive neurons. As TRPV1 expression decreases during early postnatal development (Cavanaugh et al., 2011), in adult mice, around 70% of GCaMP6s^{+} neurons were TRPV1^{+} (data not shown). Similar to findings in wild-type mice tested across the 38°C to 50°C range, we found that a growing number of cells responded to increasing temperatures from 43°C to 50°C (i.e., at the noxious heat threshold or higher), and the group of cells sensitive to lower temperature represented a nested subset of cells recruited at higher temperatures (Figure 4E). Taken individually or as a population, the enriched subpopulation of heat-sensitive neurons displayed graded responses to increasing temperature across the noxious heat range (Figure 4E). Thus, temperatures in the 43°C to 50°C range are encoded by the same strategies used to encode temperatures over the broader 38°C to 50°C range; namely, graded coding by individual neurons and by the overall population.

Encoding in the Cooling Range

To test for graded coding in the cooling range, we studied neurons that responded to all three cooling stimuli: 20°C, 15°C, and 6°C. Figure 5A shows typical responses of individual neurons at each temperature. We found that neither peak amplitude,

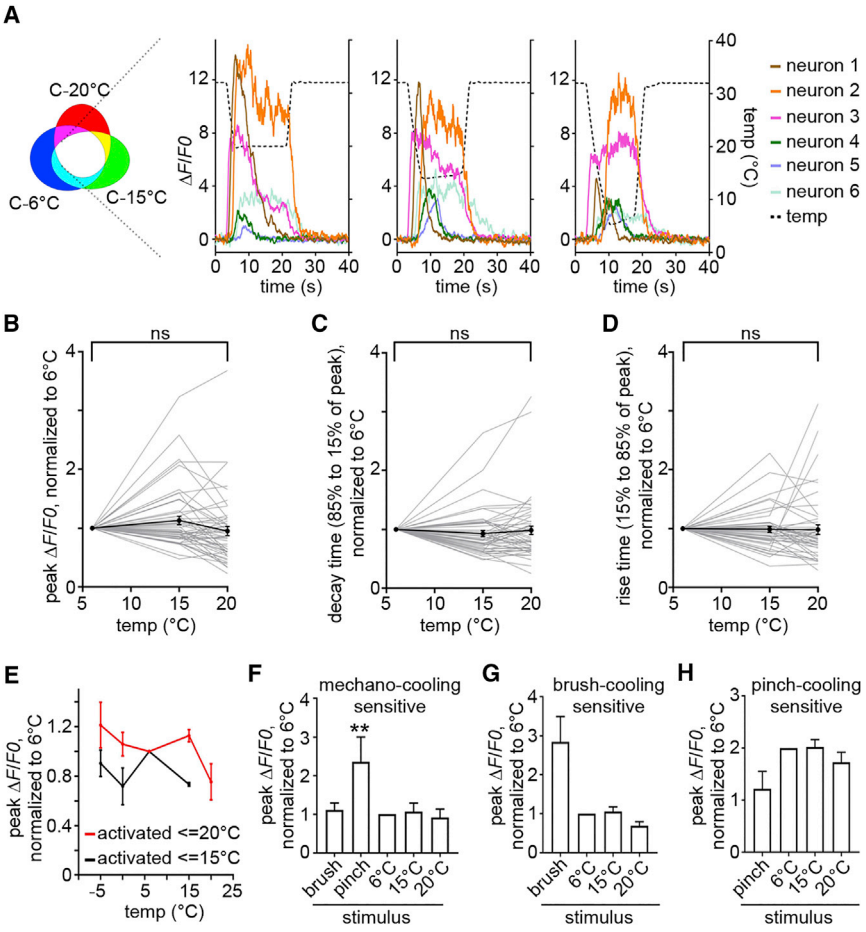

Figure 5. Cooling-Sensitive Neurons Do Not Provide Graded Coding

(A) Examples of Ca^{2+} responses of neurons sensitive to all cooling stimuli in the 20°C–6°C range (white overlap region in the Euler diagram).

(B–D) Plots of the normalized peak amplitude (B), decay time (85% to 15% of the peak, C), and rise time (15% to 85% of the peak, D) of wide-range cool/cold neurons to increasingly cooling stimuli (one-way repeated measures ANOVA test followed by Tukey's multiple comparisons test). Data are presented as mean ± SEM.

(E) The Ca^{2+} responses of a subset of cooling-sensitive neurons to extremely low temperatures, 0°C and −5°C, were not larger than those to 6°C stimulation (red for −5°C- to 20°C-responsive neurons and black for −5°C- to 15°C-responsive neurons, one-way repeated-measures ANOVA test followed by Tukey's multiple comparisons test). Data are presented as mean ± SEM.

(F–H) Normalized peak amplitude of the Ca^{2+} response of mechano-cooling sensitive neurons (F, n = 8), brush-cooling sensitive neurons (G, n = 13), and pinch-cooling sensitive neurons (H, n = 5) to mechanical and thermal stimuli. The pinch response of mechano-cooling sensitive neurons was larger than 6°C responses (one-way repeated-measures ANOVA test followed by Tukey's multiple comparisons test). Data are presented as mean ± SEM.

decay time, nor the rise time of the responses varied significantly with temperature (Figures 5A–5D).

We tested even colder temperature in a subset of experiments. Neurons that responded to 6°C showed similar sizes of responses to 0°C and −5°C (Figure 5E). Furthermore, there were no additional neurons recruited when the temperature was reduced to 0°C or −5°C, indicating lack of graded coding even at the lower temperatures and also that 6°C is a proper stimulus for noxious cold.

Importantly, the non-graded Ca^{2+} responses were not due to saturation of the signal, as evident from the observation that half of the wide-range cooling neurons also responded to mechanical stimuli, and the majority (>61%) of these neurons displayed larger Ca^{2+} responses to mechanical stimuli (Figures 5F and 5G), indicating that the Ca^{2+} responses to cooling stimuli were not saturated. Thus, cooling-sensitive neurons do not appear to utilize graded coding in the 20°C to −5°C range.

Absolute versus Relative Temperature Coding

Assuming that each neuron contributes equally to the overall output signal of a DRG, the normalized peak amplitudes of all thermoreceptors were summed to display the net output at different temperatures (Figures 6A and 6B). The net output calculated in this way and the number of activated neurons were clearly graded for temperature from 38°C to 50°C (Figure 6A) but not from 20°C to 6°C (Figure 6B). This reaffirms the graded coding of warm/heat but, taken together with the Euler diagram in Figure 3E, excludes graded coding as the basis for encoding cool/cold.

It has been reported that heating-sensitive spinal cord neurons encode absolute temperature whereas cooling-sensitive neurons encode change of temperature (Ran et al., 2016). To test whether the same pattern occurs among primary afferents, we analyzed responses that started in the return phase of our thermal stimulation protocols. For heat coding, we compared responses when the temperature was ramped from room temperature to three different higher temperatures with responses when temperature was ramped from different starting cold temperatures to neutral temperature (Figure 6C). For cold coding, we used a reverse protocol (Figure 6D). We found that heating-sensitive neurons respond to absolute temperature (i.e., during active heating) rather than the relative change in temperature (i.e., during return to baseline from cooling stimuli). Within the 4,083 neurons sampled, 2%, 4%, and 12% of neurons responded to 38°C, 43°C, and 50°C, respectively, whereas only approximately 0.5% responded during the return phase from cold temperatures (with similar step changes in temperatures; Figure 6C).

In contrast, a significant proportion of cooling-sensitive neurons responded to a decrease in temperature during the return phase from higher temperatures. Whereas 2%–3% of all neurons

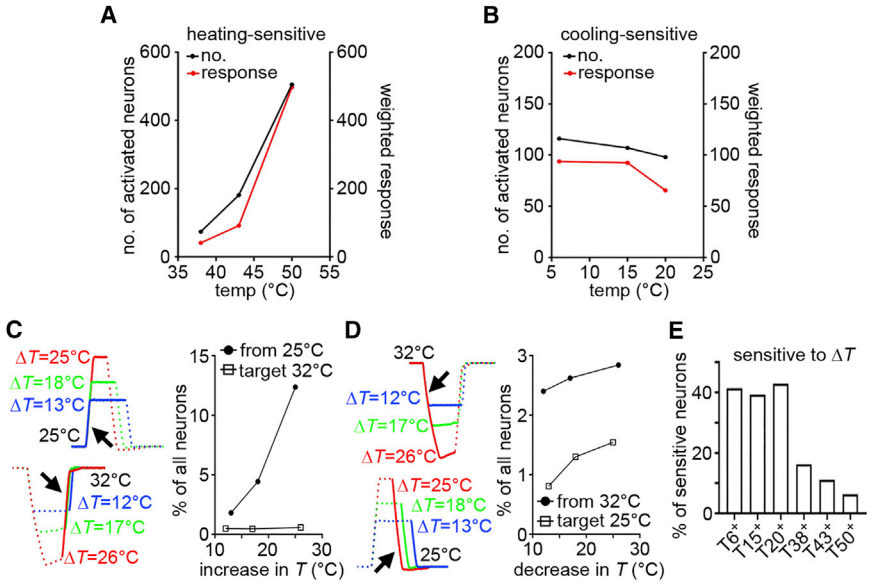

Figure 6. Cooling-Sensitive, but Not Heating-Sensitive, Neurons Responded to Change of Temperature

(A) More heating-sensitive neurons responded (left y axis), and with stronger weighted output (right y axis), as temperature was increased.

(B) Neither the number of activated cooling-sensitive neurons (left y axis) nor the weighted output (right y axis) varied as temperature was decreased.

(C) Heating-sensitive neurons primarily responded to absolute but not change in temperature. Left: protocols used for testing responses to thermal stimuli. Responses were measured during the onset and plateau phases of heating stimuli and during the return phase from cooling stimuli (arrows). Right: plots of the proportion of neurons responding to the onset and plateau phases of heating stimuli when starting from an initial temperature of 25°C (solid circle) versus those that responded to an increasing temperature change of similar degree but returning from different starting cool/cold temperatures toward a target temperature of 32°C (empty square).

(D) A significant proportion of cooling-sensitive neurons responded to a change in temperature. Left: opposite protocol to that used in (C) to test for response during the onset and plateau phases of cooling stimuli and during the return phase from heating stimuli (arrows). Right: plots of the proportion of neurons responding to the onset and plateau phases of cooling stimuli when starting from a fixed initial temperature of 32°C (solid circles) versus those that responded to a decreasing temperature change of similar degree but returning from different starting warm/hot temperatures toward a target temperature of 25°C (empty squares).

(E) Plot of the proportion of thermoceptive neurons activated by different temperatures that responded to changes in temperature.

sampled responded to cooling stimuli, a comparable proportion (0.8%–1.6%) responded during the return phase from heating stimuli (Figure 6D). Also, approximately 40% of cooling-sensitive neurons responded to the return phase from heating stimuli, whereas only 6%–16% of heating-sensitive neurons responded to the return phase from cooling stimuli (Figure 6E). These results reveal that a significant part of cooling-sensitive neurons are activated by a relative decrease in temperature, whereas heating-sensitive neurons are primarily sensitive to absolute temperature.

Distinctly Shaped Tuning Curves Support Different Coding Strategies for Heat and Cold

To explore the cellular basis for different coding strategies, we subdivided thermoceptors according to the shape of their tuning curves. A non-monotonic tuning curve is characterized by an increase and eventual decrease in response as temperature is moved away from neutral. A monotonic tuning curve is characterized by an increase and no subsequent decrease in response. Monotonic tuning curves were further divided into graded (defined by the response increasing >50% from one temperature step to the next) or steep (defined by a stable response across temperatures; i.e., <50% change across temperature steps). The vast majority (155 of 198 = 78%) of heating-sensitive neurons were monotonic, and most (131 of 155 = 85%) were graded, whereas nearly half (67 of 136 = 49%) of cooling-sensitive neurons were non-monotonic and only <20% (23 of 136 = 17%) were graded monotonic (Figure 7A). This represents a significantly different proportion of tuning curve shapes between heating- and cooling-sensitive neurons ($\chi^2 = 79.11$, $p < 1 \times 10^{-5}$). Neurons with non-monotonic tuning curves were found to have significantly larger cell bodies than neurons with monotonic tuning curves (Figure 7B), further indicating that they represent distinct populations, which may, in turn, relate to different fiber size. Notably, a sensation of painful cold at cool temperatures can be unmasked by preferential blockade of large fibers (Craig and Bushnell, 1994). Inhibition of input via certain fibers by input via other fibers relies on central circuits, but to find out whether a subtractive operation could facilitate the encoding of cold temperatures, we subtracted responses of neurons with non-monotonic tuning curves from responses of neurons with monotonic tuning curves. The result was a graded population response between 20°C and 6°C (Figure 7C), similar to the graded population response achieved through summation for temperatures between 38°C and 50°C (Figure 6A).

DISCUSSION

In contrast to the well-characterized molecular mechanisms underlying temperature detection (Patapoutian et al., 2003), our understanding of thermosensory coding at the cellular and population levels remains very incomplete. Combining *in vivo* Ca^{2+} imaging from large sets of DRG neurons with controlled thermal stimuli applied to their natural receptive field on the hind paw, we identified different strategies by which cutaneous temperature is represented by sets of distinctly tuned thermoceptive afferents. Our results emphasize that, although some cells can encode warm-hot temperatures based on their activity level, the pattern of cells activated at the population level is also important for encoding thermosensory input, especially cool-cold temperatures.

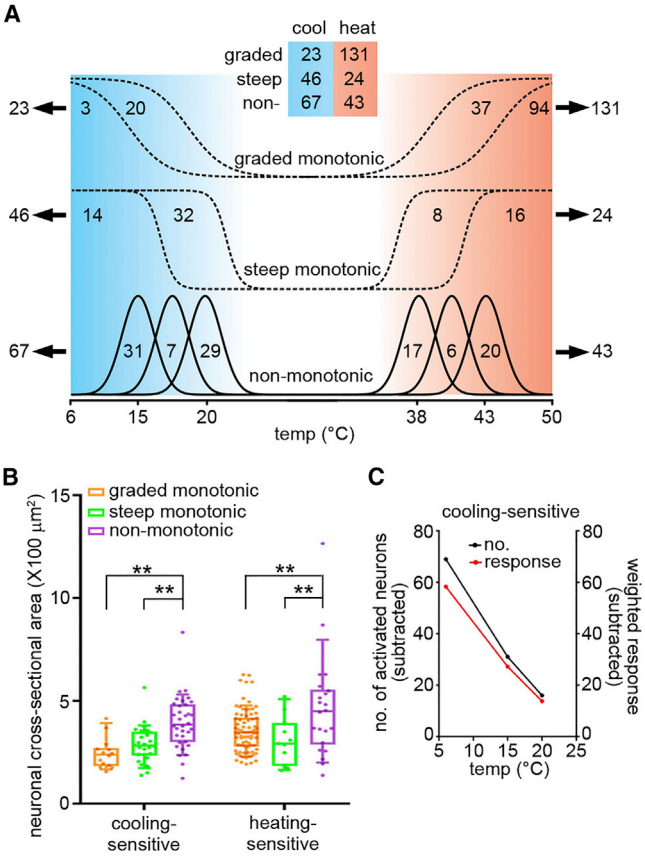

Figure 7. Heating-Sensitive and Cooling-Sensitive Neurons Had Distinct Tuning Curves

(A) The majority of heating-sensitive neurons had graded monotonic tuning curves, whereas half of the cooling-sensitive neurons had non-monotonic tuning curves ($\chi^2 = 79.11$, $p < 1 \times 10^{-5}$).

(B) In both cooling- and heating-sensitive neurons, non-monotonic neurons had larger neuronal somata than monotonic neurons (two-way ANOVA test followed by Tukey's multiple comparisons test). Boxes show quartiles, and whiskers show 10–90 percentiles.

(C) Assuming that the activity of non-monotonic cooling-sensitive neurons masks the activity of monotonic cooling-sensitive neurons, more neurons (left y axis, number of monotonic neurons minus number of non-monotonic neurons activated at each temperature) were activated at lower temperature. Also, the net weighted responses of cooling-sensitive neurons (right y axis, responses of monotonic neurons minus responses of non-monotonic neurons) were graded with decreasing temperature.

Ca^{2+} Imaging Objectively Revealed Polymodality of Sensory Neurons

Intraplantar injection of AAV9 in newborn pups was shown to provide a robust approach to specifically express exogenous genes across all classes of DRG neurons (Figures S2 and S3). The reason why we chose the postnatal viral transduction approach instead of using a transgenic mouse line, which has ubiquitous expression of GCaMP through embryonic development, is that it avoids the negative effects of Ca^{2+} buffering during embryonic development. Although GCaMP6s has relatively slower kinetics than GCaMP6f and GCaMP6m, it usually provides a higher photon budget and yields a better signal-to-noise ratio that allows more sensitive detection of activity (Broussard et al., 2014; Chen et al., 2013).

The value of *in vivo* Ca^{2+} imaging to study how neurons encode sensory input has been put into question following a report indicating that most DRG neurons were found to respond to only one type of sensory stimulus (Emery et al., 2016; Gold, 2017). One possible explanation for this result is that the numbers of cells Emery et al. (2016) reported in different functional groups were low, and this could yield misleading results for cell types that are infrequent. Here we monitored activity in several thousand neurons, which is a unique advantage of video-rate two-photon functional imaging; namely, sampling many neurons at single-neuron resolution. Our analysis reveals levels of mechano- and thermo-sensitive neurons comparable with those of electrophysiological studies (Julius and McCleskey, 2006; Koltzenburg et al., 1997; Leem et al., 1993). Although Ca^{2+} remains an indirect proxy of neuronal firing, we have shown that Ca^{2+} signals scale with the number of electrical pulses, indicating that GCaMP6s-based imaging offers a sensitive and robust approach to measure activity *in vivo* (Figures 1A–1E).

Objective estimates of the prevalence of a certain cell type remains problematic in electrophysiological studies because cells are sampled sparsely (often one at a time) and often in a biased manner (large cells or fibers are usually easier to record from). Moreover, electrophysiological studies rely heavily on the repetitive application of search stimuli, which, especially for noxious stimuli, can cause sensitization and change sensory specificity (Leem et al., 1993; Tuckett and Wei, 1987). In contrast, our imaging approach does not require extensive search stimuli, and data can be obtained from cells with no prior exposure to stimuli. What is easier to compare between imaging and electrophysiological sampling is the relative frequency of cells responding to more than one sensory modality. That said, our estimate of the proportion of cells responding to different sensory modalities is generally consistent with past estimates based on electrophysiological recordings (Cain et al., 2001; Koltzenburg et al., 1997; Leem et al., 1993; Milenkovic et al., 2014). Our finding of a high incidence of polymodal cells, particularly within the small neuron population, thus strengthens the assertion that polymodality is a prevalent phenomenon in somatosensory afferents (Perl, 1996, 2007; Zimmermann et al., 2009). Given that the experiments were performed after a laminectomy, it remains possible that top-down modulations, such as diffuse noxious inhibitory controls (Le Bars et al., 1992) or segmental inhibition (Arendt-Nielsen and Gotliebsen, 1992), were engaged, affecting the sensitivity of DRG neurons. However, this condition is not different from that in previous studies and, thus, cannot explain the difference between our results and those of Emery et al. (2016).

Different Coding Strategies for Different Sensations

The high incidence of polymodality, especially between mechano- and thermo-sensitivity, raises questions of how distinct sensations are formed. One of the main advantages of our approach of monitoring activity simultaneously in many neurons (i.e., dense sampling) is that it allowed us to identify how sets of neurons intersected in their response to different sensory modalities. This revealed that, despite the significant level of intersection (polymodality), there was also a substantial lack of overlap

between the different sets of modalities (i.e., a significant proportion of mechano- and thermo-specific neurons). This diversity at the cellular level allows for rich possibilities for coding at the population level.

Perhaps the most striking finding from our study is that heat coding appears to be clearly graded, as revealed by the intersectional and parametric analyses we performed. In other words, more heating-sensitive neurons are activated, and individual neurons are activated more strongly as thermal stimuli become increasingly hot. Although the incidence of graded coding has been observed in electrophysiological and imaging studies (Hensel and Iggo, 1971; LaMotte and Campbell, 1978; Yarmolinsky et al., 2016), evidence of graded coding at both the individual neuron and population levels could only emerge from the dense sampling made possible through imaging. On the other hand, our data preclude simple graded coding of cool-cold temperatures. Instead, our identification of distinct cell populations responsive to either a narrow or broad range of cool/cold temperatures supports a combinatorial coding scheme. Our results do not prove that activation of certain cells at cool temperatures masks the sensation of painful cold, but nor do our results rule it out; in fact, we show that a simple subtractive interaction between these two differently tuned neuron populations could underlie a viable coding scheme for cool-cold temperatures.

Information Integration from Sensory Afferents in the Spinal Cord

How the information encoded by co-activated sensory afferents is processed in the spinal dorsal horn remains a key question. Our data, combined with similar optical recordings at the spinal level, will provide avenues to establish the transfer functions at the first site of integration in the CNS. We can already compare our results with those from a recent study using population imaging in the dorsal horn to thermal stimuli (Ran et al., 2016). Ran et al. (2016) also observed that, in the heating range, spinal dorsal horn neurons encode absolute temperature, whereas, in the cooling range, neurons encode temperature change, similar to what we found in the DRGs. The CNS plays a critical role in processing input, but that processing is constrained by how sensory information is represented by primary afferent neurons. As exemplified by our study, Ca^{2+} imaging provides an invaluable tool to study those neural representations or, in other words, to uncover the neural code.

EXPERIMENTAL PROCEDURES

For a detailed description of the experimental procedures, see the Supplemental Experimental Procedures.

Animals

All experiments were performed in accordance with the regulations of the Canadian Council on Animal Care and approved by the Laval University Animal Care Committee. Pregnant C57BL/6J wild-type mice were purchased from Charles River Laboratories. $TRPV1^{Cre}$ knockin mice were purchased from The Jackson Laboratory (stock number 017769) (Cavanaugh et al., 2011). $TRPV1^{Cre}$ homozygotes were crossed with wild-type mice to yield $TRPV1^{Cre}$ heterozygote pups. Newborn pups (post-natal days 3–6) received an intraplantar injection of adeno-associated virus, subtype 9 (AAV9). Both male and female mice (6–8 weeks old) were used for imaging. Animals were maintained on a 12:12 hr light-dark cycle and housed in groups, with food and water provided *ad libitum*.

In Vivo Ca^{2+} Imaging

After laminectomy, mice were fixed on a spinal stabilization device and imaged with a home-made video-rate two-photon microscope (Laffray et al., 2011). A tunable femtosecond laser was set to 940 nm for GCaMP6s imaging. GCaMP6s was chosen because, compared with other GCaMPs (e.g., GCaMP6f), it has a higher baseline brightness, stronger sensitivity, and better signal-to-noise ratio (Chen et al., 2013), essential advantages for *in vivo* imaging and making it possible to detect neuronal activity even at a low firing level. Panoramic images of 1,000 × 500 pixels at a rate of 32 Hz (video-rate) and with a pixel size of 0.385 μm were acquired. To locate a proper imaging field, we developed a dedicated interface, allowing the users to visualize the fluorescence intensity of individual neuron in real time.

For electrical stimulation, different numbers of 5-mA current pulses (1 ms duration at 5 Hz) were delivered to the exposed sciatic nerve using a digital stimulator (PG4000A, Cygnus Technologies) and a stimulus isolation unit (A360, WPI). The in-house-acquisition software of the two-photon microscope triggered the electrical stimulator using a data acquisition card (LabJack, U3-HV).

We chose the hind paw to analyze sensory coding because it is the stimulation target for most behavioral tests and provides a large receptive field readily accessible to various stimuli. For thermal stimulation, a feedback-controlled Peltier device and a 1 × 1 cm thermal probe (TSA-II-NeuroSensory Analyzer, Medoc), large enough to cover the whole hind paw on one side, were used to deliver temperatures from 6°C to 50°C in a fast ramp-and-hold mode. The long duration allowed thermal stimuli to penetrate deep into the tissue.

For mechanical stimulation, innocuous brushing with a paintbrush and noxious pinching with serrated forceps were applied multiple times on the hind paw during the stimulus epoch. There were 3- to 5-min intervals between any two thermal or mechanical stimuli to avoid sensitization. Typical imaging fields of ~400 × 200 μm, which usually contained 70–150 neurons, were chosen by trial and error with thermal or mechanical stimulation.

Data Analysis

Acquired RAW image sequences were converted into TIFF format in ImageJ. Then the TIFF videos were registered with a custom-built MATLAB (MathWorks) function through rigid body translation alignment based on the 2D cross-correlation to correct for movement. A rectangular region of interest (ROI) in a region without any visible neuron was drawn as a background ROI. The average pixel value inside the background ROI for each frame was subtracted from every pixel in the corresponding frame to remove excess noise. Neuronal ROIs were drawn manually in the cytoplasm of visible neurons. The average fluorescence intensity of a given ROI, F_t, was measured by averaging pixel values inside the ROI. For Ca^{2+} traces, $\Delta F/F_0 = (F_t - F_0)/F_0$, where F_0 is the fluorescence value at baseline, measured as the average of the first two seconds of F_t. To avoid aberrant amplification because of small F_0 values in some neurons (e.g., low basal fluorescence), when it was <1, F_0 in the denominator, but not in the numerator, was set to 1. The resulting Ca^{2+} time series extracted from the image sequences were synchronized with thermal or mechanical stimulus data series. Processing was performed using custom functions written in MATLAB.

Positive responses were detected and measured automatically using a custom tool written in Spike2 (Cambridge Electronic Design [CED]), which provides an integrated interface to visualize and analyze traces. Raw Ca^{2+} traces were first smoothed with a 1-s temporal window. Baseline was selected from a period starting 1 s after the beginning of the recording and ending 1 s before the stimulus onset (usually 3 to 5 s in duration). Then F_b and $F_{b\text{-}max}$ were calculated as average and maximum $\Delta F/F_0$ values during baseline, respectively. A response was considered positive when the peak of the Ca^{2+} trace during stimulation was above $F_b + (F_{b\text{-}max} - F_b) \times x$, where x was a value between 2 and 3, depending on baseline stability, to provide the most reliable detection. Given the relatively slow decay of GCaMP6s, responses with a very brief duration (<0.5 s) were excluded. Although the detection algorithm was found to be highly reliable, all traces were also visually inspected to ensure that no false positive were included and no false negative missed. Peak amplitude, rise

time (from 15% to 85% of peak amplitude), and decay time (from 85% to 15% of peak amplitude) were measured for all responses using automated algorithms. For each neuron, each parameter was measured for each of the positive responses obtained over multiple trials for each stimulus and then averaged. Finally, all data were merged into a single Microsoft Excel Pivot Table database to select the proper subsets for subsequent statistical and cluster analyses.

Statistics

Data are presented as mean ± SEM unless otherwise indicated. Multiple groups were compared using one-way or two-way ANOVA followed by *post hoc* tests, as indicated in the figure legends. Two-tailed paired t tests were used to compare two groups when they were paired. The difference was considered to be significant when $p < 0.05$, and "ns" stands for "not significant."

SUPPLEMENTAL INFORMATION

Supplemental Information includes Supplemental Experimental Procedures and three figures and can be found with this article online at https://doi.org/10.1016/j.celrep.2018.04.065.

ACKNOWLEDGMENTS

We thank Modesto Peralta for behavioral tests. We thank Vivek Jayaraman, Douglas S. Kim, Loren L. Looger, and Karel Svoboda from the GENIE Project and the Janelia Research Campus, Howard Hughes Medical Institute, for sharing GCaMP6s virus. This work was supported by grants MOP 12942 to Y.D.K. and RMF 111628 to D.C.C. and Y.D.K. from the Canadian Institutes of Health Research; a Canada Research Chair on Chronic Pain and Related Brain Disorders to Y.D.K.; a team grant from the Fonds de Recherche du Québec, Nature et Technologies to D.C.C., Y.D.K., and P.D.; a Barbara Turnbull Award to Y.D.K.; a Brain Canada grant to support the Canadian Neurophotonics Platform; and grants from the Natural Sciences and Engineering Research Council of Canada (NSERC) to D.C.C. and S.A.P. (RGPIN 436168). F.W. and E.B. were partially supported by fellowships from the NSERC-funded Training Program in Biophotonics. E.B. was partially supported by fellowships from NSERC and the Multiple Sclerosis Society of Canada.

AUTHOR CONTRIBUTIONS

F.W. and Y.D.K. designed the study. F.W. conducted imaging and histochemistry experiments. E.B. and D.C.C. upgraded the microscope and thermal stimulator. E.B. and D.C.C. wrote functions for image processing. S.L.C. designed the Spike2 interface to analyze Ca^{2+} curves. S.L.C. wrote and designed algorithms to parse and analyze the data. F.W., S.L.C., S.A.P., and Y.D.K. analyzed the data. P.D. performed the fitting analysis. F.W., S.A.P., and Y.D.K. wrote the paper with help from E.B., S.L.C., and P.D. Y.D.K. and D.C.C. supervised the research.

DECLARATION OF INTERESTS

The authors declare no competing interests.

Received: May 25, 2017
Revised: February 22, 2018
Accepted: April 13, 2018
Published: May 15, 2018

REFERENCES

Arendt-Nielsen, L., and Gotliebsen, K. (1992). Segmental inhibition of laser-evoked brain potentials by ipsi- and contralaterally applied cold pressor pain. Eur. J. Appl. Physiol. Occup. Physiol. *64*, 56–61.

Basbaum, A.I., Bautista, D.M., Scherrer, G., and Julius, D. (2009). Cellular and molecular mechanisms of pain. Cell *139*, 267–284.

Beitel, R.E., and Dubner, R. (1976). Response of unmyelinated (C) polymodal nociceptors to thermal stimuli applied to monkey's face. J. Neurophysiol. *39*, 1160–1175.

Bessou, P., and Perl, E.R. (1969). Response of cutaneous sensory units with unmyelinated fibers to noxious stimuli. J. Neurophysiol. *32*, 1025–1043.

Broussard, G.J., Liang, R., and Tian, L. (2014). Monitoring activity in neural circuits with genetically encoded indicators. Front. Mol. Neurosci. *7*, 97.

Cain, D.M., Khasabov, S.G., and Simone, D.A. (2001). Response properties of mechanoreceptors and nociceptors in mouse glabrous skin: an in vivo study. J. Neurophysiol. *85*, 1561–1574.

Cavanaugh, D.J., Lee, H., Lo, L., Shields, S.D., Zylka, M.J., Basbaum, A.I., and Anderson, D.J. (2009). Distinct subsets of unmyelinated primary sensory fibers mediate behavioral responses to noxious thermal and mechanical stimuli. Proc. Natl. Acad. Sci. USA *106*, 9075–9080.

Cavanaugh, D.J., Chesler, A.T., Bráz, J.M., Shah, N.M., Julius, D., and Basbaum, A.I. (2011). Restriction of transient receptor potential vanilloid-1 to the peptidergic subset of primary afferent neurons follows its developmental downregulation in nonpeptidergic neurons. J. Neurosci. *31*, 10119–10127.

Chen, T.W., Wardill, T.J., Sun, Y., Pulver, S.R., Renninger, S.L., Baohan, A., Schreiter, E.R., Kerr, R.A., Orger, M.B., Jayaraman, V., et al. (2013). Ultrasensitive fluorescent proteins for imaging neuronal activity. Nature *499*, 295–300.

Craig, A.D. (2002). How do you feel? Interoception: the sense of the physiological condition of the body. Nat. Rev. Neurosci. *3*, 655–666.

Craig, A.D., and Bushnell, M.C. (1994). The thermal grill illusion: unmasking the burn of cold pain. Science *265*, 252–255.

Emery, E.C., Luiz, A.P., Sikandar, S., Magnúsdóttir, R., Dong, X., and Wood, J.N. (2016). In vivo characterization of distinct modality-specific subsets of somatosensory neurons using GCaMP. Sci. Adv. *2*, e1600990.

Gold, M. (2017). Comment by Michael Gold on: Allison Marin. Most DRG sensory neurons are modality-specific, not polymodal (Pain Research Forum).

Hensel, H., and Iggo, A. (1971). Analysis of cutaneous warm and cold fibres in primates. Pflugers Arch. *329*, 1–8.

Julius, D., and McCleskey, E.W. (2006). Cellular and molecular properties of primary afferent neurons. In Wall and Melzack's Textbook of Pain, 5th edition, S.B. McMahon and M. Koltsenburg, eds. (Elsevier), pp. 63–68.

Knowlton, W.M., Palkar, R., Lippoldt, E.K., McCoy, D.D., Baluch, F., Chen, J., and McKemy, D.D. (2013). A sensory-labeled line for cold: TRPM8-expressing sensory neurons define the cellular basis for cold, cold pain, and cooling-mediated analgesia. J. Neurosci. *33*, 2837–2848.

Koltzenburg, M., Stucky, C.L., and Lewin, G.R. (1997). Receptive properties of mouse sensory neurons innervating hairy skin. J. Neurophysiol. *78*, 1841–1850.

Laffray, S., Pagès, S., Dufour, H., De Koninck, P., De Koninck, Y., and Côté, D. (2011). Adaptive movement compensation for in vivo imaging of fast cellular dynamics within a moving tissue. PLoS ONE *6*, e19928.

LaMotte, R.H., and Campbell, J.N. (1978). Comparison of responses of warm and nociceptive C-fiber afferents in monkey with human judgments of thermal pain. J. Neurophysiol. *41*, 509–528.

Le Bars, D., Villanueva, L., Bouhassira, D., and Willer, J.C. (1992). Diffuse noxious inhibitory controls (DNIC) in animals and in man. Patol. Fiziol. Eksp. Ter. *4*, 55–65.

Le Pichon, C.E., and Chesler, A.T. (2014). The functional and anatomical dissection of somatosensory subpopulations using mouse genetics. Front. Neuroanat. *8*, 21.

Leem, J.W., Willis, W.D., and Chung, J.M. (1993). Cutaneous sensory receptors in the rat foot. J. Neurophysiol. *69*, 1684–1699.

Lynn, B., and Carpenter, S.E. (1982). Primary afferent units from the hairy skin of the rat hind limb. Brain Res. *238*, 29–43.

Ma, Q. (2010). Labeled lines meet and talk: population coding of somatic sensations. J. Clin. Invest. *120*, 3773–3778.

Milenkovic, N., Zhao, W.J., Walcher, J., Albert, T., Siemens, J., Lewin, G.R., and Poulet, J.F. (2014). A somatosensory circuit for cooling perception in mice. Nat. Neurosci. *17*, 1560–1566.

Molliver, D.C., Wright, D.E., Leitner, M.L., Parsadanian, A.S., Doster, K., Wen, D., Yan, Q., and Snider, W.D. (1997). IB4-binding DRG neurons switch from NGF to GDNF dependence in early postnatal life. Neuron *19*, 849–861.

Patapoutian, A., Peier, A.M., Story, G.M., and Viswanath, V. (2003). ThermoTRP channels and beyond: mechanisms of temperature sensation. Nat. Rev. Neurosci. *4*, 529–539.

Perl, E.R. (1996). Cutaneous polymodal receptors: characteristics and plasticity. Prog. Brain Res. *113*, 21–37.

Perl, E.R. (2007). Ideas about pain, a historical view. Nat. Rev. Neurosci. *8*, 71–80.

Pogorzala, L.A., Mishra, S.K., and Hoon, M.A. (2013). The cellular code for mammalian thermosensation. J. Neurosci. *33*, 5533–5541.

Prescott, S.A., and Ratté, S. (2012). Pain processing by spinal microcircuits: afferent combinatorics. Curr. Opin. Neurobiol. *22*, 631–639.

Prescott, S.A., Ma, Q., and De Koninck, Y. (2014). Normal and abnormal coding of somatosensory stimuli causing pain. Nat. Neurosci. *17*, 183–191.

Ran, C., Hoon, M.A., and Chen, X. (2016). The coding of cutaneous temperature in the spinal cord. Nat. Neurosci. *19*, 1201–1209.

Torebjörk, E. (1985). Nociceptor activation and pain. Philos. Trans. R. Soc. Lond. B Biol. Sci. *308*, 227–234.

Tuckett, R.P., and Wei, J.Y. (1987). Response to an itch-producing substance in cat. I. Cutaneous receptor populations with myelinated axons. Brain Res. *413*, 87–94.

Yang, L., Dong, F., Yang, Q., Yang, P.F., Wu, R., Wu, Q.F., Wu, D., Li, C.L., Zhong, Y.Q., Lu, Y.J., et al. (2017). FGF13 selectively regulates heat nociception by interacting with $Na_v1.7$. Neuron *93*, 806–821.e9.

Yarmolinsky, D.A., Peng, Y., Pogorzala, L.A., Rutlin, M., Hoon, M.A., and Zuker, C.S. (2016). Coding and plasticity in the mammalian thermosensory system. Neuron *92*, 1079–1092.

Zimmermann, K., Hein, A., Hager, U., Kaczmarek, J.S., Turnquist, B.P., Clapham, D.E., and Reeh, P.W. (2009). Phenotyping sensory nerve endings in vitro in the mouse. Nat. Protoc. *4*, 174–196.